THE JOURNAL OF PHYSICAL CHEMISTRY C
A JOURNAL OF THE AMERICAN CHEMICAL SOCIETY

pubs.acs.org/JPCC

Article

Seeking Out Heterogeneous Hydrogen Bonding in a Self-Assembled 2D Cocrystal of Croconic Acid and Benzimidazole on Au(111)

Daniel P. Miller, Paulo S. Costa, Jacob D. Teeter, Alexander Sinitskii, Axel Enders,* and James G. M. Hooper*

Cite This: *J. Phys. Chem. C* 2021, 125, 2403−2410

Read Online

ACCESS | Metrics & More | Article Recommendations | Supporting Information

ABSTRACT: A two-dimensional (2D) hydrogen-bonded cocrystal was synthesized from croconic acid (CA) and benzimidazole (BI) on a gold surface under ultrahigh vacuum conditions. The network domains have a 1:1 CA/BI stoichiometry, can be synthesized over a range of temperatures, and contain one-dimensional chains of molecules connected by heterogeneous hydrogen bonds. Density functional theory (DFT) computations suggest that a tautomeric salt-like structure, with deprotonated CA and protonated BI, is the most stable model, which creates heterogeneous N−H···O contacts instead of N···H−O ones. The homogeneity of the network's appearance in scanning tunneling microscopy (STM) and a habitual change in the STM features under certain tip conditions indicate that there is an equilibrium of tautomeric molecular states that may be influenced to some degree by STM stimuli. Overall, this study demonstrates how careful consideration of the precursor molecules can tune the architecture within a family of cocrystal networks and introduce desired bonding motifs that haven't been achieved by solution-based synthesis for these species, such as the heterogeneous hydrogen bonds herein.

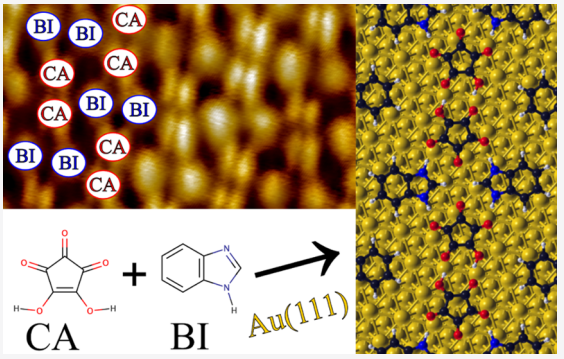

INTRODUCTION

Cocrystallization has long been used as a means of seeking out modified solid-state properties within a given set or family of materials.[1−6] Cocrystalline networks of organic molecules are often held together by intermolecular hydrogen bonds.[7−9] Where X and Y are the highly electronegative atoms or groups that participate in such hydrogen bonds, the proton's ability to switch between X−H···Y and X···H−Y positioning, typically through resonance assistance,[10] and change key crystalline and/or molecular properties has drawn much interest. Examples are the switchable direction of the electric polarization[11−13] or the reach of proton transport.[14,15] As a result, the dynamics of many proton transfer molecular materials, with croconic acid (CA) being of particular interest to this study, have been studied for their potential applications in optical instruments, ferroelectrics, and fuel cells.[7,11−13,16−21]

Traditionally, cocrystallization studies involve determining whether or not the selected precursor molecules are "compatible" to form cocrystals.[22−25] This can involve screening different possible precursors, solutions, and synthesis procedures. The inherent compatibility of the precursors to cocrystallize can therefore be difficult to assess since it is influenced by many physical variables, such as solubility, intermolecular interactions, ease of diffusion, and so on. One stratagem that has been developed is to first scrutinize such interactions in a chemical environment without solvent or mixing effects, thereby allowing the system to evolve under the guidance of the most thermodynamically stable interactions between precursor molecules; this can be achieved by letting the two molecules directly interact with each other through self-assembly under ultrahigh vacuum (UHV) on a substrate.[7−9,26,27] UHV surface deposition experiments allow the precursors to "naturally" self-assemble without solvent, but are of course influenced by the substrate itself. Au(111) substrates have often been shown, however, to have a uniform effect on the potential energy surfaces of adsorbed hydrogen-bonded molecular networks, often creating networks that would be predicted in the absence of surface-adsorbate interactions.[7,20,28] This indicates that Au(111) is a useful template for such experiments, and Au(111) further allows for the use of scanning tunneling microscopy (STM) to probe the new crystals and determine their self-assembled structures.[29−35] Even though the surface will restrict the molecular assembly by forcing it to occur at the interface, the characterization of any mixed-composition molecular network would indicate a degree

Received: September 17, 2020
Revised: December 17, 2020
Published: January 22, 2021

of thermodynamically stable interaction between the molecular precursors (vs the interactions among the separate components).

CA was recently discovered to be a room-temperature ferroelectric,[11] and has since inspired a lot of follow-up and ongoing research efforts that explore its potential use in hydrogen bond-related applications. We have found that CA deposition on Au(111) results in facile syntheses of large-domain homogeneous crystals,[20] and codeposition of CA with 3-hydroxyphenalenone (3-HPLN) on Au(111) also results in facile syntheses of crystal networks with different possible stoichiometries.[7] Our goal in this work is to further demonstrate the propensity of CA to cocrystallize with other adsorbates on a Au(111) substrate, and to demonstrate that more complex, heterogeneous hydrogen bonding patterns are feasible.

We report herein a successful cocrystallization study of CA with benzimidazole (BI). BI is, like CA and 3-HPLN, a member of the materials family of hydrogen-bonded organic ferroelectrics whose ferroelectric properties emerge from resonance-assisted hydrogen bonds that strongly couple the proton of the H-bond with the π-Electron system of the molecule, which is an essential element of having switchable molecular dipole moments.[36] We have previously investigated low-dimensional structures of CA, BI, and 3-HPLN and demonstrated that the structural motif that is at the origin of the ferroelectric behavior can be preserved in surface-supported single-component nanostructures of BI and 3-HPLN.[37] The signature structural motifs found for CA and for BI on Au(111) and their calculated binding energies are shown in Figure 1a,b. Importantly here, BI creates a different type of intermolecular hydrogen bond than CA and 3-HPLN, which is N−H···N (Figure 1b) instead of O−H···O as found for CA (Figure 1a) and 3-HPLN, and has a different size and shape than 3-HPLN. Therefore, we hypothesized that whereas CA/3-HPLN systems adopt building blocks that have 3-HPLN binding to the side of a $(CA)_2$ dimer (shown schematically in Figure 1c), CA/BI would adopt different motifs with more expansive homogeneous and heterogeneous hydrogen-bonding, since a BI molecule does not suit binding to the side of a $(CA)_2$ dimer (Figure 1d). The tactic is shown to be a success; codeposition of CA/BI on an Au(111) substrate resulted in a uniform and crystalline structure whose structure contains extended networks of mixed heterogeneous O−H···N/O···H−N (CA−BI) and homogeneous O−H···O (CA−CA) types of hydrogen bonds, both coexisting in the same network. Furthermore, we discuss how the atomic structure is best classified as an equilibrium between tautomeric molecular states, and that STM experiments appear to be capable of perturbing the equilibrium under certain tip conditions.

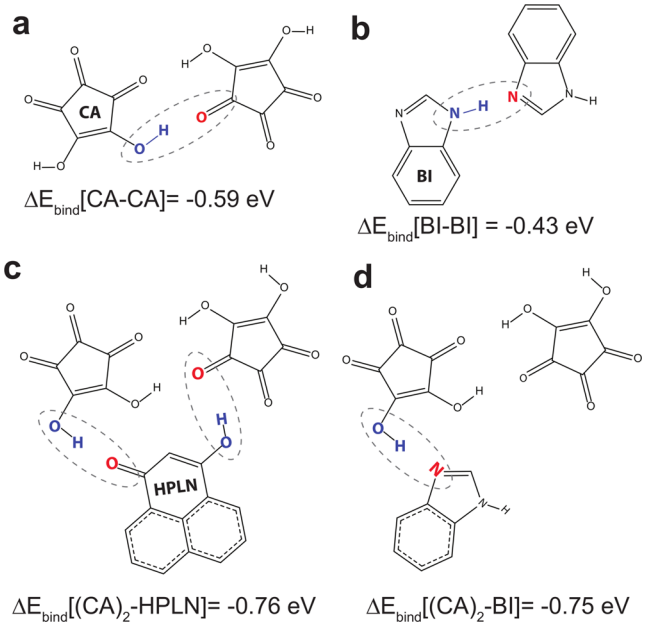

Figure 1. Computed structures and binding energies, ΔE_{bind}, of (a) a CA dimer, $(CA)_2$, and (b) a BI dimer, $(BI)_2$; ΔE_{bind} is computed as $\Delta E_{bind}(X - Y) = E(X) - E(Y)$, where $E(X)$ is the computed total energy of molecule X. (c) A sketch of the manner in which a 3-HPLN molecule was found to bind to CA in CA/3-HPLN cocrystals.[7] (d) A sketch of the optimized geometry of a BI molecule binding to the side of a CA dimer.

METHODS

Experimental investigations were performed in UHV at a base pressure of 1×10^{-10} millibars. A gold metal substrate of (111) orientation was prepared in situ by repeated cycles of Ar+ ion sputtering and subsequent annealing at approximately 873 K. Characteristic of the clean Au(111) surface is the herringbone surface reconstruction, which has been checked with STM. The herringbone reconstruction is easily visible in the STM images in this study as ripples underneath the molecular adlayers. In the vacuum system, the molecules were thermally evaporated from a home-built four-pocket Knudsen cell onto the substrates, which were held at room temperature during the film growth. The deposition rate was about 0.03−0.5 monolayers per minute, depending on the desired coverage. For cocrystallization, CA and BI were codeposited simultaneously at crucible temperatures that were pre-calibrated to give approximately the same evaporation rates for both of the species. The pressure during deposition is typically 5×10^{-8} millibars. After film growth, the samples were transferred in situ into an Omicron low-temperature STM, where they were imaged at 77 K substrate temperature. The STM was operated with electrochemically etched tungsten tips.

Density functional theory (DFT) calculations were carried out using the ADF software[38,39] for molecular gas-phase CA/BI clusters and the VASP software[40,41] package for periodic models. The revPBE functional[42−44] was used for all of the electronic structures and geometries discussed in the main text, and combined with a post-SCF dispersion correction[45] (revPBE-D3). All of the ADF calculations used the triple-zeta Slater-type basis set with polarization functions (TZP) from the ADF basis set library, and the results were compared with other density functionals and methods (see the SI). The VASP calculations employed the projector augmented wave (PAW) method to treat the core states[46,47] and a plane-wave basis set with an energy cutoff of 500 eV. Further computational details for the periodic calculations, including the different functionals that were checked and the setup of the surface/adsorbate systems, are provided in the SI. The Vesta and Xcrysden packages were used to generate some of the graphics and structures in this work.[48,49]

RESULTS AND DISCUSSION

CA/BI Experimental STM Imaging. The single-component networks that have been imaged for BI and CA alone on

https://dx.doi.org/10.1021/acs.jpcc.0c08483
J. Phys. Chem. C 2021, 125, 2403−2410

Au(111) are shown in Figure 2a,b. CA will self-assemble into porous honeycomb networks (Figure 2b), and BI forms long zipper-like chains that pack closely together (Figure 2a),[21,37] incorporating the building blocks shown below each image in Figure 2. An STM image of a layer consisting of CA and BI, which were codeposited on Au(111) at room temperature, is shown in Figure 3a. Since BI and CA are similar in size, it is difficult to differentiate one molecule from the other in the STM image. However, it is plainly seen that the crystal structure that is observed when both ingredients are codeposited differs significantly from the single-component networks.

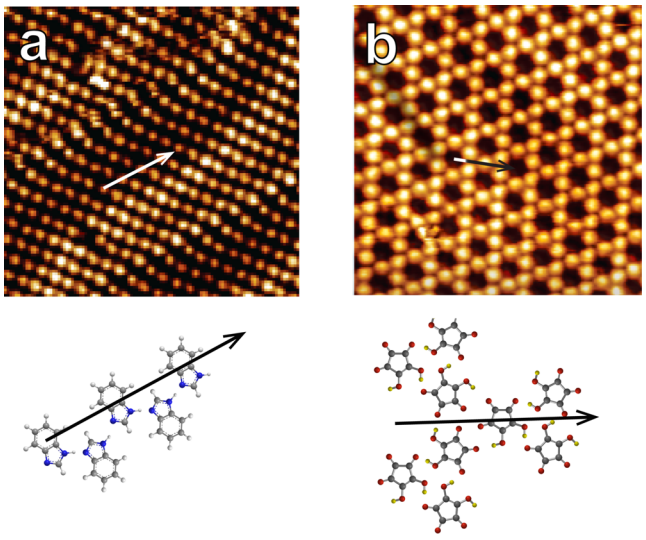

Figure 2. STM images of self-assembled single-component two-dimensional (2D) molecular structures on an Au(111) substrate: (a) BI, wherein the Au(111) substrate herringbone reconstruction pattern is visible through the monolayer, and (b) CA. The building blocks of each self-assembled monolayer are shown below the STM images.

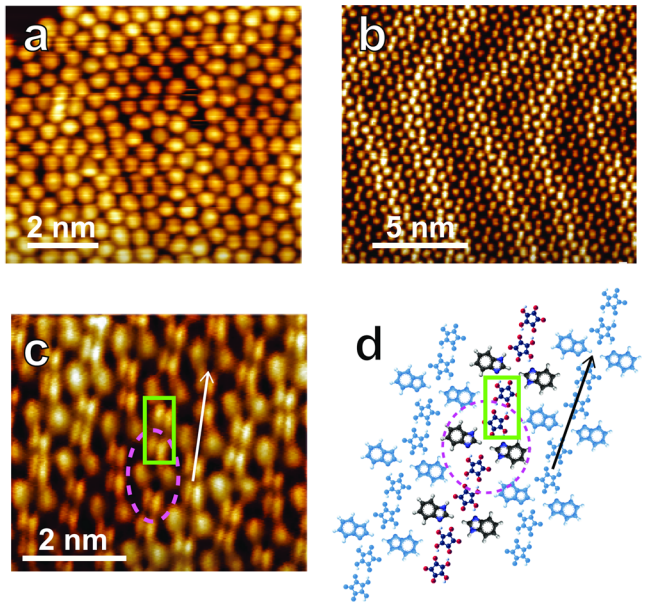

Figure 3. STM images of self-assembled 2D molecular structures on an Au(111) substrate. (a) BI and CA in a disordered phase; (b) annealed BI and CA to form an ordered crystal structure, with Au(111) substrate reconstruction patterning visible; (c) Close view of BI and CA in the ordered phase, with there being a distinct visible difference between the two different molecules; (d) the building blocks of the ordered self-assembled monolayer of CA/BI on Au(111).

The disorganized structure of the deposited films of CA and BI at room temperature has no discernible periodic order. However, annealing this disorganized phase lightly (50 °C) triggers molecular reorganization on the surface and the ordered periodic cocrystal structure shown in Figure 3b emerges. Thus, a consistent and reproducible recipe for creating a mixed phase of CA and BI on Au(111) was discovered. The new phase was uniform and ubiquitous throughout the sample and there were no indications of the single-molecule phases from either independent ingredient molecule (see the SI for example images with less magnification). From this, we may conclude that both ingredient molecules are coming together to create a particularly stable new 2D crystal structure. It appears from the STM images that the codeposited CA/BI network is constructed from cross-shaped building blocks, such as the one highlighted in Figure 3c with a dashed oval. To some extent, these tetramers vaguely resemble the hydrogen-bonded CA/3-HPLN tetramers reported previously.[7]

While the appearances of BI and CA are similar in an STM image, under certain tip conditions and voltages, the molecules appear to differentiate themselves (see Figure 3c). It can be seen that while some molecules retain their circular shape, some molecules resemble two parallel ovals. We can discern from this that each tetramer building block consists of two pairs of different molecules, and then assume a $(CA)_2(BI)_2$ stoichiometry. With this in mind, an intuitive model for the recurring $(CA)_2(BI)_2$ motif was built and is shown in Figure 4a. As expected, this $(CA)_2(BI)_2$ tetramer is distinct from the building block we observed recently in CA/3-HPLN networks[7] in how it does not contain the previously found CA dimer (Figure 1a), but rather the $(CA)_2$ dimer emerges in the network to connect adjacent $(CA)_2(BI)_2$ building blocks together, see the proposed periodic structure in Figure 4b. This demonstrates the second realization of the project's goals: to tune CA's cocrystalline structure such that the intermolecular hydrogen bonds are not contained within a tetramer building block but are carried on in a long-rage periodic pattern, which, in this case, consists of alternating CA−CA and CA-BI hydrogen bond bridges along infinite one-dimensional chains. The orientations of the molecules along these chains, in symmetric dimers and tetramers, cancel out any potential overall network dipole moment and so, similar to pure CA and CA/3-HPLN networks on Au(111),[7,20] the CA/BI cocrystal ground state structure is not spontaneously polarized as it is in bulk crystal CA.[11] Neighboring H-bonded chains, which are differently shaded in the model in Figure 3d, are densely packed but are not otherwise connected by any H-bond.

CA/BI Computational Insights. Dispersion-corrected DFT computations were used to study the nature of the binding within the proposed structural model (Figure 4b). It was found that the $(CA)_2(BI)_2$ tetramer spontaneously tautomerizes when the geometries of both the isolated tetramer cluster and periodic network models were optimized (see Figure 4a/b). The tautomerization corresponds with a proton transfer from each CA to a nearby BI, and creates two N−H hydrogen bond donor groups per BI (cation) molecule instead of only one. The optimized salt-like model (**2**) mimics

https://dx.doi.org/10.1021/acs.jpcc.0c08483
J. Phys. Chem. C 2021, 125, 2403−2410

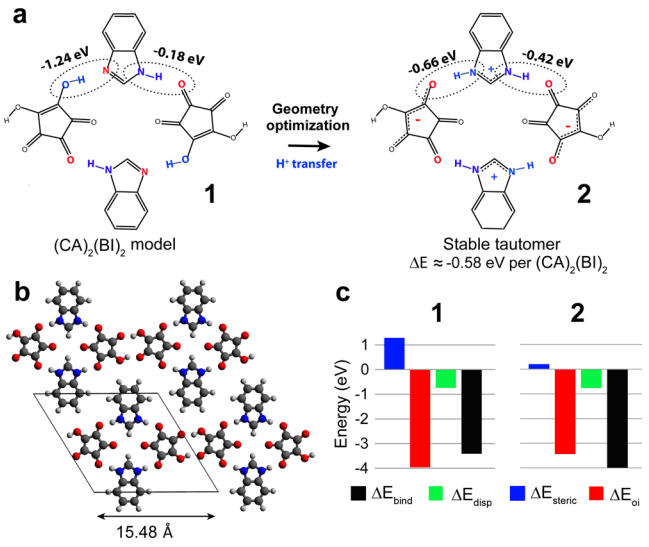

Figure 4. (a) A sketch of the proposed $(CA)_2(BI)_2$ tetramer model (**1**). When its geometry is optimized with DFT, it spontaneously tautomerizes to the structure shown to the right (**2**). The energy values show estimates of the relative stabilization that each hydrogen bond type contributes to the tetramer's binding energy as a result of charge-transfer within and among the molecular fragments. (b) Atomic structure of the optimized periodic $(CA)_2(BI)_2$ network. (c) A comparison between the total binding energies, $\Delta E_{bind} = E(CA_2BI_2) - 2*E(CA) - 2*E(BI)$, of the **1** and **2** $(CA)_2(BI)_2$ clusters, as well as their decomposition within an ETS-NOCV framework, which can be used to express ΔE_{bind} as $\Delta E_{bind} = \Delta E_{disp} + \Delta E_{steric} + \Delta E_{oi}$.

computational models of the previously reported CA/3-HPLN cocrystal networks[7] and was reproduced with other DFT methodologies (see the SI for details) and with Hartree-Fock and MP2 wavefunction-based methods. The binding energy, ΔE_{bind}, of the isolated neutral molecules coming together to form the **2** $(CA)_2(BI)_2$ tetramer building block is computed to be −3.99 eV per $(CA)_2(BI)_2$ unit (−1.00 eV per molecule), while a ΔE_{bind} value of −4.46 eV is found with the periodic model. The difference in ΔE_{bind} between the cluster and periodic models, −0.47 eV per $(CA)_2(BI)_2$, is largely accounted for by the periodic models having additional hydrogen bonding contributions from the $(CA)_2$ dimer units that bridge adjacent $(CA)_2(BI)_2$ tetramers; an isolated $(CA)_2$ dimer has a ΔE_{bind} value of −0.59 eV per $(CA)_2$ (Figure 1a). The computed reaction energy of forming the cocrystal network from the homogeneous "parent" networks of CA and BI, i.e., $[(CA)_3]_n + [(BI)_2]_n \rightarrow [(CA)_2(BI)_2]_n$, is computed to be favorable at −1.73 eV per $(CA)_2(BI)_2$. The predicted stability of the mixed $(CA)_2(BI)_2$ network can be recovered from a simple model that sums up all the interaction energies from pairs of hydrogen-bonded molecules within each network, which sums up to −0.63 eV per $(CA)_2(BI)_2$. This confirms that part of the driving force for cocrystallization, within DFT, is to strengthen the interactions between adjacent (hydrogen-bonded) molecules.

By using geometry constraints to fix the O−H···N distances within the tetramers at the values they adopt in $(CA)_1(BI)_1$ dimers (to keep the **1** motifs intact during geometry optimizations), it was estimated that the tautomerization contributes significantly, at roughly 15%, to the total binding energy of the tetramer. It should be noted, however, that the energy differences between **1** and **2** can change significantly with different DFT functionals and with other methodologies (like Hartree-Fock and MP2, which are less favoring, relatively speaking, of the tautomer), and also it can be noted that the local symmetry within the imaged tetramer building blocks does sometimes appear as could be expected from the less-symmetric hydrogen-bonding in **1**. Since **2** is energetically favored in all of the periodic models, we used the ETS-NOCV method[50] to study the key differences between the **1** and **2** motifs by decomposing the DFT binding energy of the $(CA)_2(BI)_2$ tetramer into $\Delta E_{bind} = \Delta E_{disp} + \Delta E_{steric} + \Delta E_{oi}$, where ΔE_{disp} includes the post-SCF dispersion corrections between molecules, ΔE_{oi} includes the attractive interactions that come about from allowing inter- and intra-molecular charge flow between the fragments' molecular orbitals, and ΔE_{steric} includes everything else (such as Pauli repulsion and electrostatic interactions between "frozen" molecular fragments, and a geometry deformation energy).

The bond-energy decomposition results are presented in Figure 4c. It can be seen that **1** and **2** indeed have distinct signatures with this representation of ΔE_{bind}. The ΔE_{oi} term is relatively diminished in **2**, while the ΔE_{steric} term is strengthened. A more in-depth ETS-NOCV analysis (i.e., a decomposition of ΔE_{oi}) confirms that the diminished ΔE_{oi} of **2** correlates with weaker contributions from the intermolecular hydrogen bonding; the energy contributions for each type of hydrogen bond are indicated in Figure 4a. Despite its weaker overall ΔE_{oi}, the tautomerization curiously still strengthens the charge-transfer character of the (weakest) N−H···O hydrogen bond from **1**; this relates with the resonance-stabilized partial atomic positive charges on the BI nitrogen atoms. The electrostatic interactions included in the ΔE_{steric} term of **2** further compensate and overpower the apparent diminished strength of the hydrogen bonding to ΔE_{oi}. The stability of **2** in DFT is thus attributed, primarily, to the molecules' resonance structures and intermolecular electrostatic interactions. This corroborates our speculation about the importance of such intermolecular electrostatic interactions in stabilizing CA/3-HPLN networks.[7] Furthermore, this suggests that future efforts to synthesize cocrystals with non-tautomerized hydrogen-bonded networks would benefit from being designed so that they embellish the relative importance of ΔE_{oi}'s contribution to ΔE_{bind} or diminish the role of ΔE_{steric}.

Regardless of the tautomer structure, the proposed $[(CA)_2(BI)_2]_n$ structure has no net dipole moment (see the sketch of molecular dipole moments within the **1**-based model in Figure 5), and we therefore do not expect CA/BI networks to exhibit significant ferroelectricity. Intermolecular proton transfers can be imagined within the $[(CA)_2(BI)_2]_n$ model which create substantial spontaneous polarization, such as the structure shown in Figure 5b, but such a structure is not a stable local minimum on the DFT potential energy surface, and when geometry constraints are used to optimize a model of it, it is over 1.2 eV per $(CA)_2(BI)_2$ unit less stable than the model network in Figure 5a. The stability of a non-polar ground state clearly indicates that the $[(CA)_2(BI)_2]_n$ structure is not as potentially ferroelectric as the single-component two-dimensional BI networks. Furthermore, it is likely that attempts to polarize such a network structure with an external chemical potential would induce more limited proton transfer mechanisms with much smaller perturbations to the overall polarization vector, like a toggling of N−H···O and N···H−O bonds.

The $[(CA)_2(BI)_2]_n$ model network was also modeled over a four-layer Au(111) slab with a $(2\sqrt{7} \times 2\sqrt{7})$ overlay; this cell

https://dx.doi.org/10.1021/acs.jpcc.0c08483
J. Phys. Chem. C 2021, 125, 2403−2410

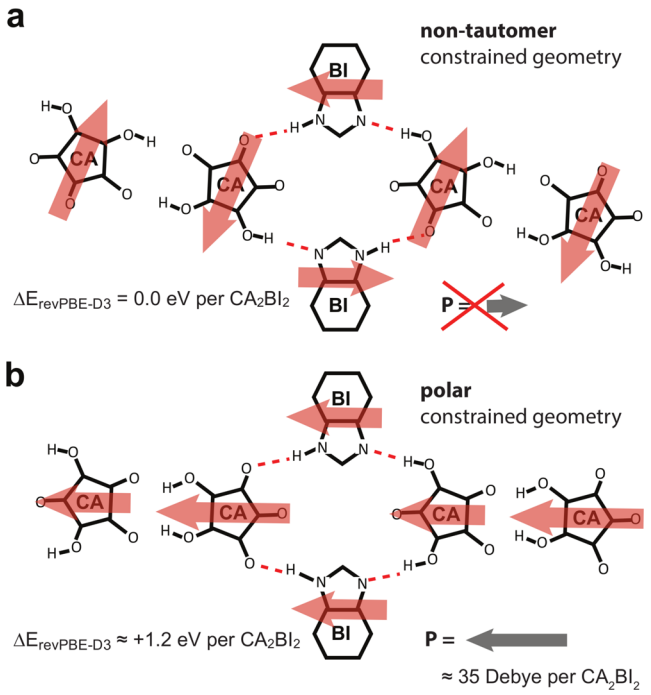

Figure 5. A potential structural transformation of the $[(CA)_2(BI)_2]_n$ model network that aligns all of the molecular dipole moments in the same direction. The **1**-based model of the network is shown in (a), wherein the molecular dipole moments are depicted with arrows to show how they cancel out (resulting in a zero net polarization vector, P). A constructed polar network is shown in (b), but note that this network is not a minimum on the DFT potential energy surface (the central $(CA)_2(BI)_2$ tetramer tautomerizes upon geometry optimization).

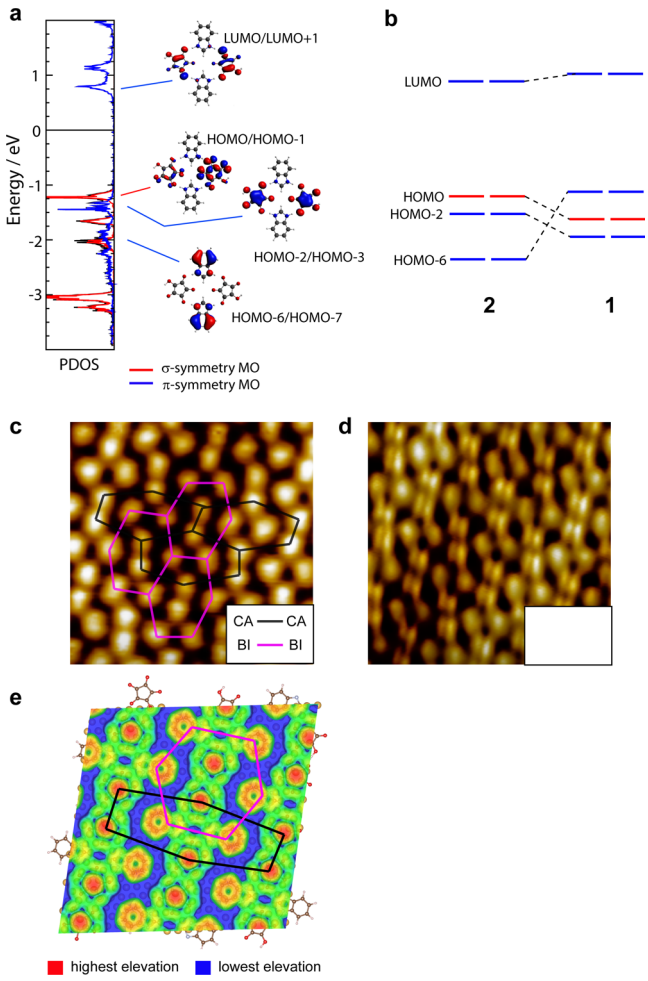

Figure 6. (a) Projected densities of states of the optimized $[(CA)_2(BI)_2]_n$/Au(111) network onto (blue line) atomic s, px, and py-character states (σ-symmetry electronic states) and onto (red line) pz-character atomic states (π-symmetry electronic states). The molecular orbitals (MO's) from isolated $(CA)_2(BI)_2$ clusters which best match up with the peaks in the PDOS are shown to the right. In (b), we show, schematically, how the relative energies of these molecular orbitals are affected by the tautomerization. (c, d) STM images of CA and BI adsorbed to Au(111), scanned at −2.3 and −1.7 V, respectively [(d) are also shown in Figure 3c)]. A double-oval feature shows up in (d) that is not present in (c). (e) Corrugation profile of the partial charge density generated from the local density of states within a −2.3 to 0.0 eV energy window from the Fermi energy for the DFT-optimized $[(CA)_2(BI)_2]_n$/Au(111) model system.

was chosen since it allows for near-optimal intermolecular distances along the molecular chains as determined from gas-phase network models (albeit compressed by roughly 0.1 Å per cell). The **2**-based structure was again recovered as the most energetically stable model structure, and the charge-transfer within it is clearly evidenced by the computed Bader charges that are assigned to each molecule's constituent atoms (−0.84*e* on CA and +0.84*e* on BI). The binding energy is computed to be −8.91 eV per $(CA)_2(BI)_2$ unit, which can readily be decomposed into a −4.76 eV per $(CA)_2(BI)_2$ unit contribution that comes from the interaction of the network with the surface, and a −4.15 eV per $(CA)_2(BI)_2$ unit contribution that comes from the formation of the $[(CA)_2(BI)_2]_n$ network from the isolated molecules. Analysis of the charge density difference plots confirms that its most prominent features conform to an asymmetric redistribution of charge along the hydrogen bonds (see the SI), which is a hallmark of hydrogen-bonded networks. The projected densities of states onto select molecular orbitals are shown in Figure 6a and confirm that the molecular orbitals of the $(CA)_2(BI)_2$ tetramer building block are easily recognized (the positions of the peaks which correspond to selected frontier molecular orbitals are labeled). This is all consistent with the overall weak influence of the substrate on the intermolecular interactions, despite the strong overall dispersion-driven bond strength, and corroborates that the networks which we have imaged here can possibly be synthesized on semiconducting substrates which have a similar relatively inert influence on the molecule−molecule interactions.

Considering the possibility of toggling between the hydrogen bond types with STM, we revisit the habitual occurrence of a "double-oval" feature in STM that was both seen (Figure 6d, reproduced from Figure 3c) and not seen (Figure 6c) during data collection. We noted that the charge density generated from the local density of states within −2.3 eV of the Fermi level for the DFT-optimized model network (shown in Figure 6e) agrees fairly well with the overall appearance of the measured STM images in Figure 6c,d; the CA and BI molecules take on distorted hexagonal sublattices, with one of them, in this case CA (colored black in Figure 6e), being far more distorted than the other. The double-oval feature also belongs to the molecular sublattice with the shortest intermolecular distances (estimated to be 0.6 vs 0.8 nm from the STM images). Since the CA−CA and BI−BI distances are

https://dx.doi.org/10.1021/acs.jpcc.0c08483
J. Phys. Chem. C 2021, 125, 2403−2410

estimated to be 0.7 and 0.9 nm, respectively, in our molecular model, we assign the double-oval feature as a CA molecule. With this assignment, it is interesting to note that the dark areas in the center of the tetramers from the STM imaging would correspond with areas of low charge density above BI's five-membered rings, which serves as another example of parts of molecules being invisible in STM experiments.

By defining a narrower energy window such that only the CA molecular states are sampled, for example, with a −1.7 eV energy interval below the Fermi level, we could generate local charge densities with very large differences in "contrast" at each site (CA vs BI), as shown in the SI. This is consistent with the computed densities of states in Figure 6a, wherein the highest occupied molecular states are localized on CA. Since experiments did not detect any such differences in the molecular contrast at different voltages, we interpret this as a suggestion that the two states are at an equilibrium over the timescale of the STM measurement, by invoking the Tersoff-Hamann approximation[51] and assuming that such a chemical effect within the adsorbate would not be overridden by other substrate effects. Figure 6b shows how the tautomerization process results in a rearrangement of the molecular orbitals near the Fermi level. The drastic change in the local densities of states upon tautomerization suggests that STM imaging may noticeably change if the STM tip were to perturb the tautomer-based equilibrium (because of the changes to the molecular orbitals near the Fermi level),[52] and it is tempting to relate the differences between the CA^- and CA molecular orbitals with the differences that were observed in Figures 6c/d. On one hand, it is worth noting, as shown in the ESI, that the double-oval motif was also seen at a positive bias of +1.0 V and that observable changes in molecular images upon deprotonation are known.[52] On the other hand, we cannot rule out that the observed effect is an artifact of some other combined substrate/tip/network aspect of the experiment (see, as an example, Figure S16 in the ESI, which shows an STM scan image that exhibits clear vertical-axis switching from single-lobe motifs to double-lobe motifs). Nonetheless, the modeling shows the potential for what would constitute a response within the $[(CA)_2(BI)_2]_n$ network to an external STM stimulus, demonstrating that although the Au(111) substrate does not appear to inhibit the self-assembly of these molecules, it, or another substrate, can influence the hydrogen bonding arrangement.

CONCLUSIONS

A rational design of a tuned cocrystal molecular architecture that contains molecules from two types of room-temperature ferroelectrics, CA and BI, is presented. CA was successfully codeposited with BI on an Au(111) substrate, and it was found that the CA/BI networks can always be coaxed, requiring at most a mild annealing, to adopt a well-defined cocrystalline network with a $[(CA)_2(BI)_2]_n$ stoichiometry. The crystal structure resembles, in its homogeneity, our recently reported CA/3-HPLN cocrystal network,[7] but it adopts a differently assembled tetramer-based building block that allows for extended hydrogen-bonding along chains rather than closed hydrogen-bonded molecular loops. Computations show that the binding of the molecules to the surface drives a significant portion of the overall binding energy, but that the molecules are nonetheless energetically driven via the expected hydrogen bonding interactions to assemble on their own. Computations further suggest that a tautomer-based salt structure, a result of spontaneous proton transfer from O−H···N to O···H−N, is heavily favored by the models because of increased intermolecular electrostatic and dispersion interactions, but, concurrently, the DFT-favored tautomer structure weakens the intermolecular charge-transfer component of the hydrogen bonding. An inspection of experimental and simulated STM topographies suggests that STM imaging is possibly perturbing the balance between tautomer states. This makes us wonder whether or not the different signatures of the salt-like (**2**) and unperturbed (**1**) molecular states can be incorporated into future synthetic stratagems.

Most importantly, this study shows that cocrystalline hydrogen-bonded networks can reliably be created via solvent-free surface deposition studies and that they bind together as could be expected and predicted from computations and chemical intuition. This demonstrates the usefulness of STM in testing compatible cocrystal precursors without having to search for the proper solvent and mixing method. We hope this inspires further studies to seek out deposited molecular networks that adopt functional structures and properties.

ASSOCIATED CONTENT

Supporting Information

The Supporting Information is available free of charge at https://pubs.acs.org/doi/10.1021/acs.jpcc.0c08483.

It contains information about previous CA cocrystallization attempts, additional STM images, and additional computational data, including calculated binding energies of molecular cluster models, electron density profiles of CA/BI models on Au(111), and descriptions of the tautomer structure models on Au(111) (PDF)

AUTHOR INFORMATION

Corresponding Authors

Axel Enders − *Department of Physics & Astronomy, University of Nebraska, Lincoln, Nebraska 68588-0299, United States; Physikalisches Institut, Universität Bayreuth, 95440 Bayreuth, Germany;* orcid.org/0000-0003-3671-5406; Email: axel.enders@uni-bayreuth.de

James G. M. Hooper − *Department of Theoretical Chemistry, Faculty of Chemistry, Jagiellonian University, 30-060 Krakow, Poland;* orcid.org/0000-0003-3859-6172; Email: james.hooper@uj.edu.pl

Authors

Daniel P. Miller − *Department of Chemistry, Hofstra University, Hempstead, New York 11549, United States;* orcid.org/0000-0003-1507-2667

Paulo S. Costa − *Department of Physics & Astronomy, University of Nebraska, Lincoln, Nebraska 68588-0299, United States*

Jacob D. Teeter − *Department of Chemistry, University of Nebraska, Lincoln, Nebraska 68588-0304, United States*

Alexander Sinitskii − *Department of Chemistry, University of Nebraska, Lincoln, Nebraska 68588-0304, United States;* orcid.org/0000-0002-8688-3451

Complete contact information is available at: https://pubs.acs.org/10.1021/acs.jpcc.0c08483

Notes

The authors declare no competing financial interest.

https://dx.doi.org/10.1021/acs.jpcc.0c08483
J. Phys. Chem. C 2021, 125, 2403−2410

■ ACKNOWLEDGMENTS

D.P.M. thanks Hofstra University for start-up funding. J.G.M.H. thanks the Ministry of Polish Science for financial support via an "Outstanding Young Scientist" Award. J.G.M.H. and D.P.M. thank the PLgrid infrastructure in Poland and the Center of Computational Research and their employees at University at Buffalo, SUNY for computational support.

■ REFERENCES

(1) El-Gizawy, S. A.; Osman, M. A.; Arafa, M. F.; Maghraby, G. M. E. Aerosil as a novel co-crystal co-former for improving the dissolution rate of hydrochlorothiazide. *Int. J. Pharm.* **2015**, *478*, 773−778.
(2) Hipps, K. W.; Scudiero, L.; Barlow, D. E.; Cooke, M. P. A Self-Organized 2-Dimensional Bifunctional Structure Formed by Supramolecular Design. *J. Am. Chem. Soc.* **2002**, *124*, 2126−2127.
(3) Childs, S. L.; Zaworotko, M. J. The Reemergence of Cocrystals: The Crystal Clear Writing Is on the Wall Introduction to Virtual Special Issue on Pharmaceutical Cocrystals. *Cryst. Growth Des.* **2009**, *9*, 4208−4211.
(4) Bouju, X.; Mattioli, C.; Franc, G.; Pujol, A.; Gourdon, A. Bicomponent Supramolecular Architectures at the Vacuum-Solid Interface. *Chem. Rev.* **2017**, *117*, 1407−1444.
(5) Yang, X.-Q.; Yi, Z.-Y.; Wang, S.-F.; Chen, T.; Wang, D. Construction of 2D extended cocrystals on the Au(111) surface via I...aldehyde halogen bonds. *Chem. Commun.* **2020**, *56*, 3539−3542.
(6) Kampschulte, L.; Werblowsky, T. L.; Kishore, R. S. K.; Schmittel, M.; Heckl, W. M.; Lackinger, M. Thermodynamical Equilibrium of Binary Supramolecular Networks at the Liquid-Solid Interface. *J. Am. Chem. Soc.* **2008**, *130*, 8502−8507.
(7) Kunkel, D. A.; Hooper, J.; Bradley, B.; Schlueter, L.; Rasmussen, T.; Costa, P.; Beniwal, S.; Ducharme, S.; Zurek, E.; Enders, A. 2D Cocrystallization from H-Bonded Organic Ferroelectrics. The. *J. Phys. Chem. Lett.* **2016**, *7*, 435−440.
(8) Cañas-Ventura, M. E.; Xiao, W.; Wasserfallen, D.; Müllen, K.; Brune, H.; Barth, J. V.; Fasel, R. Self-Assembly of Periodic Bicomponent Wires and Ribbons. *Angew. Chem., Int. Ed.* **2007**, *46*, 1814−1818.
(9) Theobald, J. A.; Oxtoby, N. S.; Phillips, M. A.; Champness, N. R.; Beton, P. H. Controlling molecular deposition and layer structure with supramolecular surface assemblies. *Nature* **2003**, *424*, 1029−1031.
(10) Dannenberg, J. J. The Nature of the Hydrogen Bond: Outline of a Comprehensive Hydrogen Bond Theory. *J. Am. Chem. Soc.* **2010**, *132*, 3229.
(11) Horiuchi, S.; Tokunaga, Y.; Giovannetti, G.; Picozzi, S.; Itoh, H.; Shimano, R.; Kumai, R.; Tokura, Y. Above-room-temperature ferroelectricity in a single-component molecular crystal. *Nature* **2010**, *463*, 789−792.
(12) Horiuchi, S.; Kobayashi, K.; Kumai, R.; Ishibashi, S. Proton tautomerism for strong polarization switching. *Nat. Commun.* **2017**, *8*, No. 14426.
(13) Horiuchi, S.; Kobayashi, K.; Kumai, R.; Minami, N.; Kagawa, F.; Tokura, Y. Quantum ferroelectricity in charge-transfer complex crystals. *Nat. Commun.* **2015**, *6*, No. 7469.
(14) Day, T. J. F.; Schmitt, U. W.; Voth, G. A. The Mechanism of Hydrated Proton Transport in Water. *J. Am. Chem. Soc.* **2000**, *122*, 12027−12028.
(15) Wolke, C. T.; Fournier, J. A.; Dzugan, L. C.; Fagiani, M. R.; Odbadrakh, T. T.; Knorke, H.; Jordan, K. D.; McCoy, A. B.; Asmis, K. R.; Johnson, M. A. Spectroscopic snapshots of the proton-transfer mechanism in water. *Science* **2016**, *354*, 1131−1135.
(16) Bolla, G.; Dong, H.; Zhen, Y.; Wang, Z.; Hu, W. Organic cocrystals: the development of ferroelectric properties. *Sci. China Mater.* **2016**, *59*, 523−530.
(17) Di Sante, D.; Stroppa, A.; Picozzi, S. Structural, electronic and ferroelectric properties of croconic acid crystal: a DFT study. *Phys. Chem. Chem. Phys.* **2012**, *14*, 14673−14681.
(18) Cai, Y.; Luo, S.; Zhu, Z.; Gu, H. Ferroelectric mechanism of croconic acid: A first-principles and Monte Carlo study. *J. Chem. Phys.* **2013**, *139*, No. 044702.
(19) Jiang, X.; Lu, H.; Yin, Y.; Zhang, X.; Wang, X.; Yu, L.; Ahmadi, Z.; Costa, P. S.; DiChiara, A. D.; Cheng, X.; et al. Room temperature ferroelectricity in continuous croconic acid thin films. *Appl. Phys. Lett.* **2016**, *109*, No. 102902.
(20) Hooper, J.; Kunkel, D. A.; Zurek, E.; Enders, A. Interplay between Hydrogen Bonding, Epitaxy, and Charge Transfer in the Self-Assembly of Croconic Acid on Au(111) and Ag(111). *J. Phys. Chem. C* **2015**, *119*, 26429−26437.
(21) Kunkel, D. A.; Hooper, J.; Simpson, S.; Rojas, G. A.; Ducharme, S.; Usher, T.; Zurek, E.; Enders, A. Proton transfer in surface-stabilized chiral motifs of croconic acid. *Phys. Rev. B* **2013**, *87*, No. 041402(R).
(22) Lei, S.; Surin, M.; Tahara, K.; Adisoejoso, J.; Lazzaroni, R.; Tobe, Y.; De Feyter, S. Programmable Hierarchical Three-Component 2D Assembly at a Liquid-Solid Interface: Recognition, Selection, and Transformation. *Nano Lett.* **2008**, *8*, 2541−2546.
(23) Yoshimoto, S.; Higa, N.; Itaya, K. Two-Dimensional Supramolecular Organization of Copper Octaethylporphyrin and Cobalt Phthalocyanine on Au(111): Molecular Assembly Control at an Electrochemical Interface. *J. Am. Chem. Soc.* **2004**, *126*, 8540−8545.
(24) Plass, K. E.; Engle, K. M.; Cychosz, K. A.; Matzger, A. J. Large-Periodicity Two-Dimensional Crystals by Cocrystallization. *Nano Lett.* **2006**, *6*, 1178−1183.
(25) Wei, Y.; Tong, W.; Zimmt, M. B. Self-Assembly of Patterned Monolayers with Nanometer Features: Molecular Selection Based on Dipole Interactions and Chain Length. *J. Am. Chem. Soc.* **2008**, *130*, 3399−3405.
(26) Barrena, E.; de Oteyza, D. G.; Dosch, H.; Wakayama, Y. 2D Supramolecular Self-Assembly of Binary Organic Monolayers. *ChemPhysChem* **2007**, *8*, 1915−1918.
(27) Rojas, G. A.; Ganesh, P.; Kelly, S. J.; Sumpter, B. G.; Schlueter, J. A.; Maksymovych, P. Ionic Disproportionation of Charge Transfer Salt Driven by Surface Epitaxy. *J. Phys. Chem. C* **2013**, *117*, 19402−19408.
(28) Kunkel, D. A.; Hooper, J.; Simpson, S.; Miller, D. P.; Routaboul, L.; Braunstein, P.; Doudin, B.; Beniwal, S.; Dowben, P.; Skomski, R.; et al. Self-assembly of strongly dipolar molecules on metal surfaces. *J. Chem. Phys.* **2015**, *142*, No. 101921.
(29) Bao, M.; Wei, X.; Cai, L.; Sun, Q.; Liu, Z.; Xu, W. Self-assembly of melem on Au(111) and Ag(111): the origin of two different hydrogen bonding configurations. *Phys. Chem. Chem. Phys.* **2017**, *19*, 18704−18708.
(30) De Marchi, F.; Galeotti, G.; Simenas, M.; Ji, P.; Chi, L.; Tornau, E. E.; Pezzella, A.; MacLeod, J.; Ebrahimi, M.; Rosei, F. Self-assembly of 5,6-dihydroxyindole-2-carboxylic acid: polymorphism of a eumelanin building block on Au(111). *Nanoscale* **2019**, *11*, 5422−5428.
(31) Steiner, C.; Gliemann, B. D.; Meinhardt, U.; Gurrath, M.; Meyer, B.; Kivala, M.; Maier, S. Self-Assembly and Stability of Hydrogen-Bonded Networks of Bridged Triphenylamines on Au(111) and Cu(111). *J. Phys. Chem. C* **2015**, *119*, 25945−25955.
(32) Leasor, C.; Goshinsky, K.; Chen, K.-H.; Li, Z. Probing Molecular Nanostructures of Aromatic Terephthalic Acids Triggered by Intermolecular Hydrogen Bonds and Electrochemical Potential. *Langmuir* **2019**, *35*, 13259−13267.
(33) Smykalla, L.; Shukrynau, P.; Mende, C.; Rüffer, T.; Lang, H.; Hietschold, M. Interplay of hydrogen bonding and molecule substrate interaction in self-assembled adlayer structures of a hydroxyphenyl-substituted porphyrin. *Surf. Sci.* **2014**, *628*, 132−140.
(34) Quardokus, R. C.; Wasio, N. A.; Brown, R. D.; Christie, J. A.; Henderson, K. W.; Forrest, R. P.; Lent, C. S.; Corcelli, S. A.; Alex Kandel, S. Hydrogen-bonded clusters of ferrocenedicarboxylic acid on Au(111) are initially formed in solution. *J. Chem. Phys.* **2015**, *142*, No. 101927.
(35) Schmidt, N.; Enache, M.; Maggini, L.; Havenith, R. W.; Bonifazi, D.; Stöhr, M. Coverage-Controlled Polymorphism of H-

https://dx.doi.org/10.1021/acs.jpcc.0c08483
J. Phys. Chem. C 2021, 125, 2403−2410

Bonded Networks on Au(111). *J. Phys. Chem. C* **2019**, *123*, 7151−7157.
(36) Horiuchi, S.; Kagawa, F.; Hatahara, K.; Kobayashi, K.; Kumai, R.; Murakami, Y.; Tokura, Y. Above-room-temperature ferroelectricity and antiferroelectricity in benzimidazoles. *Nat. Commun.* **2012**, *3*, No. 1308.
(37) Costa, P. S.; Miller, D. P.; Teeter, J. D.; Beniwal, S.; Zurek, E.; Sinitskii, A.; Hooper, J.; Enders, A. Structure and Proton-Transfer Mechanism in One-Dimensional Chains of Benzimidazoles. *J. Phys. Chem. C* **2016**, *120*, 5804−5809.
(38) te Velde, G.; Bickelhaupt, F. M.; Baerends, E. J.; Fonseca Guerra, C.; van Gisbergen, S. J. A.; Snijders, J. G.; Ziegler, T. Chemistry with ADF. *J. Comput. Chem.* **2001**, *22*, 931−967.
(39) Baerends, E. J.; Autschbach, J.; Bérces, A.; Bickelhaupt, F. M.; Bo, C.; Boerrigter, P. M.; Cavallo, L.; Chong, D. P.; Deng, L.; Dickson, R. M. et al. *ADF2010.01*; SCM: Amsterdam, 2010.
(40) Kresse, G.; Hafner, J. Ab Initio Molecular Dynamics for Liquid Metals. *Phys. Rev. B* **1993**, *47*, 558−561.
(41) Kresse, G.; Furthmuller, J. Efficient Iterative Schemes for Ab Initio Total-energy Calculations Using a Plane-wave Basis Set. *Phys. Rev. B* **1996**, *54*, 11169−11186.
(42) Perdew, J. P.; Burke, K.; Wang, Y. Generalized gradient approximation for the exchange-correlation hole of a many-electron system. *Phys. Rev. B* **1996**, *54*, 891.
(43) Zhang, Y.; Yang, W. Comment on a Generalized Gradient Approximation Made Simple. *Phys. Rev. Lett.* **1998**, *80*, 890.
(44) Perdew, J. P.; Burke, K.; Ernzerhof, M. A Reply to the Comment by Yingkai Zhang and Weitao Yang. *Phys. Rev. Lett.* **1998**, *80*, 891.
(45) Grimme, S.; Antony, J.; Ehrlich, S.; Krieg, H. A consistent and accurate ab initio parametrization of density functional dispersion correction (DFT-D) for the 94 elements H-Pu. *J. Chem. Phys.* **2010**, *132*, No. 154104.
(46) Blöchl, P. Projector Augmented-wave Method. *Phys. Rev. B* **1994**, *50*, 17953.
(47) Kresse, G.; Joubert, D. From Ultrasoft Pseudopotentials to the Projector Augmented-wave Method. *Phys. Rev. B* **1999**, *59*, 1758−1775.
(48) Momma, K.; Izumi, F. *VESTA3* for three-dimensional visualization of crystal, volumetric and morphology data. *J. Appl. Crystallogr.* **2011**, *44*, 1272−1276.
(49) Kokalj, A. Computer Graphics and Graphical User Interfaces as Tools in Simulations of Matter at the Atomic Scale. *Comp. Mater. Sci.* **2003**, *28*, 155−168.
(50) Mitoraj, M. P.; Michalak, A.; Ziegler, T. A Combined Charge and Energy Decomposition Scheme for Bond Analysis. *J. Chem. Theory Comput.* **2009**, *5*, 962−975.
(51) Tersoff, J.; Hamann, D. R. Theory of the scanning tunneling microscope. *Phys. Rev. B* **1985**, *31*, 805−813.
(52) Auwärter, W.; Seufert, K.; Bischoff, F.; Ecija, D.; Vijayaraghavan, S.; Joshi, S.; Klappenberger, F.; Samudrala, N.; Barth, J. V. A surface-anchored molecular four-level conductance switch based on single proton transfer. *Nat. Nanotechnol.* **2012**, *7*, 41−46.

https://dx.doi.org/10.1021/acs.jpcc.0c08483
J. Phys. Chem. C 2021, 125, 2403−2410